THE ASTROPHYSICAL JOURNAL, 411:137–152, 1993 July 1

ABUNDANCES OF H II REGIONS IN EARLY-TYPE SPIRAL GALAXIES[1]

M. S. OEY AND R. C. KENNICUTT, JR.
Steward Observatory, University of Arizona, Tucson, AZ 85721
Received 1992 August 25; accepted 1993 January 4

ABSTRACT

We present an abundance study of H II regions in 15 Sa to Sb galaxies. We find that the metal abundances of the H II regions are systematically higher than those in Sc and later type galaxies, although this effect is not a function of Hubble type only. The distribution of reddening values is similar to late-type spirals, indicating that the dust levels associated with our sample of H II regions are not unusually high. This implies that the systematic changes in H II region luminosity along the Hubble sequence are due to intrinsic differences in the properties of the gas and ionizing OB associations, rather than to differences in extinction. Our data also suggest that the abundance gradients in early-type galaxies may generally be flatter than in Sc galaxies. The metallicities within our sample exhibit no correlation with galaxy mass, suggesting that mass is not the only factor driving the observed gas-phase abundances among luminous ($M_B < -20$) spiral galaxies. We have also computed photoionization models of metal-rich (0.5–3 $Z_\odot$) H II regions, in order to evaluate the reliability of the Pagel & Edmunds R_{23} empirical abundance parameter in this abundance range. The results indicate that R_{23} provides a valuable means of ranking relative abundances in this regime, but systematic variations in other parameters, most notably nebular density and stellar effective temperature, introduce significant uncertainties into the abundance scales.

Subject headings: galaxies: abundances — galaxies: spiral — H II regions

1. INTRODUCTION

Observations of giant H II regions provide accessible and important probes of the physical conditions in other galaxies. They furnish information about the interstellar medium from which they are formed, as well as stellar populations to which they give birth. One of the most important parameters derived from extragalactic H II regions is the determination of elemental abundances (e.g., Dinerstein 1990; Pagel & Edmunds 1981), which constrain models of stellar evolution, galactic evolution, and big bang nucleosynthesis.

Unfortunately most published spectroscopy of extragalactic H II regions has been limited to the brightest objects in the nearest galaxies. These occur almost exclusively in gas-rich, late-type spiral galaxies (Sbc–Im), which contain giant H II regions with Hα luminosities of up to 10^{40} ergs s^{-1} (Kennicutt 1988). In contrast, H II regions in progressively earlier type galaxies exhibit smaller dimensions and correspondingly fainter luminosities. The brightest H II regions in a typical Sa galaxy may be two orders of magnitude fainter than those in an Sc galaxy (e.g., Caldwell et al. 1991; Shields 1990; Kennicutt 1988). This has led to an understandable observational selection in favor of late-type galaxies, and consequently most of our empirical understanding of the chemical evolution of disks is limited to a restricted subset of galaxy types and interstellar environments.

This paper presents the first results from a spectroscopic survey of H II regions in early-type (Sa to Sb) galaxies. The main goal of this investigation is to extend the study of gas-phase disk abundances to the full range of morphological types. A systematic correlation between metallicity and earlier morphological type has been suggested by previous investigators (e.g., Edmunds & Pagel 1984; Smith 1975; Searle 1971), but these studies focused mainly on galaxies of type Sbc or later. Garnett & Shields (1987) investigated the metallicities of H II regions in the nearby Sab galaxy M81 and found its abundance patterns to be similar to those in later type galaxies. Garnett & Shields did find evidence, on the other hand, for a correlation between mean abundance and galaxy luminosity or mass. Since galaxies of a given morphological type show a large dispersion in mean abundances (e.g., Zaritsky, Elston, & Hill 1990; Díaz 1989), data for a larger sample of early-type systems can provide a much more sensitive test for these trends.

A second motivation for our study is to better understand the physical origin of the dramatic changes in H II region properties along the Hubble sequence. The faintness of the H II regions in early-type spirals could reflect a proportional decrease in star formation rates in these regions, but the effect could also arise from systematic changes in extinction or the stellar initial mass function with morphological type. As demonstrated later, the nebular spectra provide valuable diagnostics for discriminating between these alternatives.

2. OBSERVATIONS

We report spectra for 67 H II regions in a sample of 15 galaxies ranging in type from Sa to Sb, as listed in the *Revised Shapley-Ames Catalog* (Sandage & Tammann 1987, hereafter RSA). Besides morphological type, selection criteria included small distance, low inclination, and the presence of observable H II regions, as determined from inspection of Hα images. In addition, the sample was confined to field galaxies, to avoid possible effects of cluster environment (Shields, Skillman, & Kennicutt 1991). Although it was our original intention to obtain a uniform sampling of Hubble types over the range S0/a–Sb, the faintness of the targets in the earliest-type spirals limited our coverage of those systems. The galaxy sample is summarized in Table 1. The first few columns provide fundamental identification parameters, with type and recession

[1] Observations reported here were obtained with the Multiple Mirror Telescope, a facility operated jointly by the Smithsonian Institution and the University of Arizona.

TABLE 1

THE GALAXY SAMPLE

NGC (1)	Type[a] (2)	v_0[a] (km s^{-1}) (3)	R.A. (4)	Decl. (5)	i[b] (6)	pa[b] (7)	log $2R_E$[c] 0.1 (8)	log D_0[c] 0.1 (9)	$M^{0,ia}_{B_T}$ (10)
772.....	Sb(rs)I	2645	01^{h}56^{m}35^s	18°46.0	52°	130°	...	1.83	−22.94
1068.....	Sb(rs)II	1234	02 40 07	−00 13.5	38	52[d]	1.23	1.85	−22.58
2460.....	Sab(s)	1593	07 52 36	60 29.0	46	40[e]	0.85	1.48	−20.27
2841.....	Sb	714	09 18 35	51 11.3	64	150	1.30	1.85	−21.18
3031.....	Sb(r)I-II	124	09 51 30	69 18.3	59[f]	332[f]	1.85	2.38	−20.75
3351.....	SBb(r)II	641	10 41 19	11 58.1	48	15[g]	1.28[g]	1.86	−20.31
3368.....	Sab(s)II	758	10 44 08	12 05.1	45	147[e]	1.35	1.83	−21.06
3623.....	Sa(s)II	675	11 16 19	13 21.9	71	−10[e]	1.38	1.91	−21.13
4258.....	Sb(s)II	520	12 16 29	47 35.0	69	−30	1.75	2.20	−21.70
4736.....	RSab(s)	345	12 48 32	41 23.6	35	122	1.30[g]	2.04	−20.46
4826.....	Sab(s)II	350	12 54 17	21 57.1	58	115	1.38	1.94	−20.26
5005.....	Sb(s)II	1042	13 08 37	37 19.4	62	155	1.15	1.68	−21.43
5701.....	(PR)SBa	1424	14 36 41	05 34.8	18	88[e]	1.20	1.69	−20.15
6384.....	Sb(r)I.2	1735	17 29 59	07 05.8	46	34	1.40	1.81	−21.93
7331.....	Sb(rs)I-II	1114	22 34 47	34 09.5	71	170	1.33	1.98	−22.25

[a] From RSA; $M^{0,i}_{B_T}$ corrected to $H_0 = 75$ km s^{-1}/Mpc.
[b] From Huchtmeier & Richter 1989, unless otherwise indicated.
[c] From RC2, unless otherwise indicated.
[d] From Nishimura et al. 1984.
[e] Visually estimated from CCD image.
[f] From Rots 1974.
[g] From McCall 1982.

velocity in columns (2) and (3), and coordinates (epoch 1950) in columns (4) and (5). The inclination and position angles are listed in columns (6) and (7), and effective and isophotal diameters in columns (8) and (9), respectively. Finally, total integrated luminosity is given in column (10).

The extreme faintness of the H II regions in early-type spiral galaxies posed a major challenge to obtaining their spectra. Most of the objects presented here have Hβ fluxes of order 10^{-14} to 10^{-16} ergs s^{-1} cm^{-2}. For reference, this range is roughly 10–1000 times fainter than the brightest H II regions in the Sc galaxy M101. Blind offsets, which were required for all but the brightest H II regions, were measured from narrow-band Hα images of the host galaxies. These were obtained at the Steward Observatory 2.3 m telescope, using an f/2.25 focal reducer CCD camera. Offsets from the galactic nuclei or nearby foreground stars were measured by centroiding in a 6.″0 box on each H II region, providing accuracy to better than 1″. For a few galaxies with brighter H II regions, we used positions from the H II region atlas of Hodge & Kennicutt (1982) and visually positioned the objects on the slit.

The spectroscopic observations were obtained with the Red Channel CCD spectrograph on the Multiple Mirror Telescope (MMT) during 4.5 nights in 1990 January, March, and June. A 600 gpm grating blazed at 4800 Å was used with a 2″ × 180″ slit, which provided spectral coverage from the [O II] $\lambda\lambda$3726, 3729 to [O III] λ5007 oxygen emission lines, at a resolution of 10 Å FWHM. The detector used was a thinned and UV-flooded Texas Instruments 800 × 800 pixel CCD. The CCD was read out with 30 μm pixels, which correspond to 0.″63 spatially and 3.2 Å along the dispersion. The long slit allowed for an accurate local background subtraction, extremely important for these faint H II regions. The instrument was frequently rotated to a position angle which would allow two or more H II regions to be measured simultaneously, within constraints imposed by minimizing atmospheric differential refraction. Total integration times ranged from 600 to 3600 s, depending on the brightness and excitation of the H II regions.

Most of the objects in our sample are not only faint, but also exhibit low excitation spectra, so the only bright emission features over our spectral range are the Balmer lines, the [O II] $\lambda\lambda$3726, 3729 doublet, and in the higher excitation objects, [O III] $\lambda\lambda$4959, 5007 and [Ne III] λ3869. Whenever possible, sufficient integration time was obtained to provide high signal-to-noise measurements of at least three Balmer lines (Hβ, Hγ, Hδ), so that an accurate reddening correction could be derived. Two typical spectra are presented in Figure 1, showing a high-excitation example (1*a*), and one with low-excitation (1*b*).

Spectra were obtained for three or more H II regions in each program galaxy. Whenever possible at least five, and as many as 12, H II regions were observed. The primary selection criteria were flux and galactocentric radius, such that regions spanning the maximum range of radius were observed, within the limits set by the faintness of the objects. During data reduction many observations with insufficient signal-to-noise were discarded, and the actual number of H II regions in the final sample ranged from one to 11 per galaxy. It is notable that forbidden-line emission was detected in every H II region studied. As discussed in § 4, this excludes the presence of ultra-metal-rich, cool H II regions in our sample.

Initial data reduction followed routine procedures, including bias and flat-field corrections and photometric calibration, using the CCD reduction programs in the IRAF software package. Flux calibration was performed on the Hayes & Latham (1975) system, using standard stars selected from Massey et al. (1988). One-dimensional spectra were extracted with apertures of 4″–20″ (× 2″ slit width), depending on the seeing and size of the object, with typical apertures being roughly 10″. The apparent sizes of the H II regions varied, with FWHM angular extents of typically several arcseconds. Line fluxes and equivalent widths were measured by direct numerical integration, using the one-dimensional spectrum package in IRAF.

The relevant line fluxes were measured and corrected for reddening and Balmer absorption in the underlying stellar

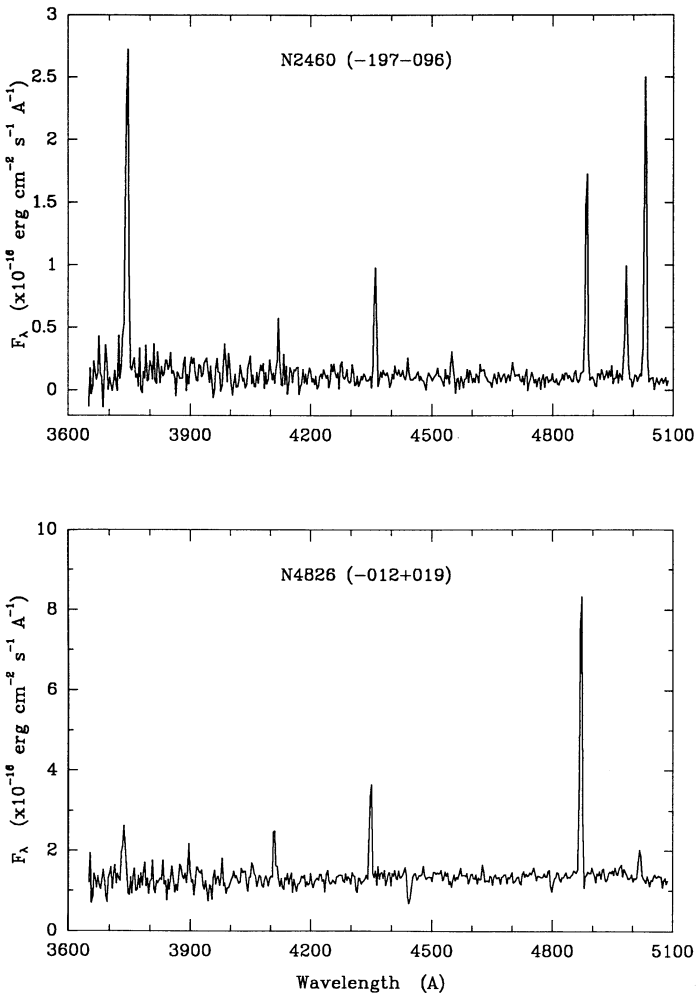

FIG. 1.—Examples of typical spectra from our sample, displaying the approximate range in excitation for our objects. Panel (*a*) shows high excitation in [O III] λλ4959, 5007 and [O II] λλ3726, 3729 (unresolved); (*b*) shows low excitation in these lines compared to Hβ (λ4861). These spectra also show sample emission line fluxes of order 10^{-16} ergs s^{-1} cm^{-2}.

continuum. Many of the H II regions in our sample exhibit a strong continuum, so Balmer absorption-line corrections were essential in order to avoid large systematic errors in the reddening determination. The average Balmer absorption equivalent width was derived by fitting the relative intensities Hβ, Hγ, and Hδ to the theoretical values compiled in Osterbrock (1989), with the reddening law of Schild (1977), and assuming a constant absorption-line equivalent width for all three lines. An average electron temperature of 8000 K was assumed, and the solutions were derived numerically by Newton-Raphson iteration. In cases where Hδ was measured with high signal-to-noise, reddening values were determined independently from the Hβ/Hγ and Hγ/Hδ ratios, and averaged with weighting proportional to the signal-to-noise at Hβ and Hγ. Given the large errors and dispersion (±4.2 Å) in the resulting absorption equivalent widths for individual H II regions, the mean value of 2 Å was adopted for all objects. This mean excludes values which deviated by more than 3 σ. Our adopted value of 2 Å was also derived by McCall, Rybski, & Shields (1985, hereafter MRS), based on measurements of H II regions in mostly late-type spirals.

The reddening values were then recomputed for each object with the 2 Å absorption correction. Again, wherever possible, the two solutions obtained from the three Balmer lines were averaged, weighted by the signal-to-noise ratios at Hβ and Hγ. In some cases the computed reddening was negative, in which case it was set to 0. The observed emission-line ratios were then corrected for this reddening. This selective correction causes the mean reddening of the sample to be slightly higher than before correction, but does not affect the interpretation of our results.

Spectra were obtained for roughly 100 H II regions. For this analysis we discarded spectra with low signal-to-noise (< 5.5 in Hγ), or objects which were too heavily contaminated by underlying stellar continuum. These discarded data had excitation properties similar to those of the high-quality data. The analysis of the remaining spectra for 67 H II regions which passed all quality tests is presented in this paper. Our selection criteria assure that uncertainties in the derived abundances will be dominated by systematic effects in the excitation-abundance calibration, and not by errors in the observed excitation values.

3. RESULTS

Table 2 summarizes the corrected spectra of the H II regions in our sample. Column (1) of the table lists the H II region by its position with respect to the galactic nucleus in units of arcseconds east and north, respectively. These positions are quoted for identification purposes only, since not all are measured with the same degree of accuracy. Column (2) lists the measured visual extinction, as described above, and columns (3) and (4) list the measured equivalent width and error for the Hβ emission line. The reddening-corrected strengths relative to Hβ, of the [O II] λλ3726, 3729 doublet (not resolved in our data), and the [O III] λλ4959, 5007 pair are listed in columns (5) and (7), respectively. In both cases the line strengths refer to the sum of the two doublet components; for [O III] this was assumed to be 1.335 times the flux of the 5007 Å line. Columns (6) and (8) of the table give the estimated logarithmic uncertainty in the line ratios, including both the signal-to-noise in the spectrum and errors in the aperture extraction and reddening correction. A full listing of observed and dereddened line fluxes will be published in a future paper, along with additional observations of these H II regions with spectral coverage extending to 10,000 Å.

3.1. *Reddening and Extinction*

Our data allow us to test whether unusual levels of extinction are partly responsible for the systematically low luminosities observed in these H II regions in early-type galaxies. The excitation itself, however, is not expected to vary significantly due to dust absorption for most H II regions (Mathis 1986). Figure 2 compares the distribution of visual extinctions derived for our study (upper panel) with a sample of 137 H II regions, mostly in late-type spirals and irregular galaxies, compiled by Kennicutt, Keel, & Blaha (1989, lower panel). Most of the latter are from the survey of MRS and were derived using the same Balmer absorption correction and extinction law as were assumed in our analysis. In this comparison we restricted our own sample to those H II regions for which we obtained spectra with high signal-to-noise in the three Balmer lines Hβ, Hγ, Hδ.

Figure 2 shows that the typical extinction in the H II regions in our sample of Sa–Sb galaxies is comparable to or even lower than that for the comparison sample of largely late-type spirals. Indeed the mean value for our sample (A_V = 0.6 mag) is

TABLE 2

OBSERVATIONS

Object (1)	A_V (mag) (2)	$W(H\beta)$ (Å) (3)	Error (4)	$\log \frac{[O\ II]}{H\beta}$ (5)	Error (6)	$\log \frac{[O\ III]}{H\beta}$ (7)	Error (8)
N772(+024+060)	2.84	49.2	2.1	0.11	0.04	−0.85	0.33
N1068(−025−036)	0.94	88.8	1.1	−0.06	0.05	−0.59	0.17
N1068(−025−032)	1.28	15.5	0.4	−0.06	0.05	−0.62	0.19
N1068(−013−008)	2.00	29.3	0.4	−0.21	0.07	−0.60	0.18
N1068(−032+001)	0.00	16.0	0.4	0.06	0.05	0.02	0.04
N1069(−021+020)	0.16	23.1	1.6	0.03	0.06	−0.14	0.08
N1068(+019+010)	1.04	45.8	0.3	−0.22	0.07	−0.18	0.07
N1068(+023+017)	0.48	18.0	0.8	−0.06	0.07	−0.99	0.47
N1068(−019+009)	0.00	29.1	1.6	−0.22	0.09	−0.49	0.15
N2460(−017+003)	0.00	7.0	0.7	0.07	0.09	0.06	0.06
N2460(−197−096)	0.00	127.9	7.1	0.28	0.04	0.31	0.03
N2841(−042+086)	0.00	35.0	3.9	−0.20	0.10	−0.74	0.36
N3031(+107−291)	0.30	75.8	3.6	0.29	0.03	0.07	0.04
N3351(+023+067)	0.00	14.5	1.1	−0.50	0.19	−0.98	0.52
N3351(+000+068)	0.47	45.9	4.0	−0.38	0.15	−1.04	0.63
N3351(−058−135)	0.30	107.6	2.7	−0.02	0.05	−0.57	0.17
N3351(−088−026)	1.32	133.4	4.2	−0.20	0.07	−0.91	0.37
N3351(−105−086)	0.26	90.7	2.8	0.05	0.04	−0.52	0.15
N3351(−001+006)	3.17	33.6	1.3	−0.36	0.11	−1.27	0.86
N3368(+054−024)	0.51	32.1	0.7	−0.03	0.05	−0.73	0.24
N3368(+054−026)	0.24	37.9	1.6	−0.13	0.07	−0.73	0.25
N3368(−052+025)	1.87	30.7	1.3	0.31	0.03	−0.57	0.17
N3623(−003−086)	1.59	11.7	0.6	0.09	0.05	−0.76	0.28
N4258(−318+183)	1.08	77.0	4.6	0.62	0.02	−0.01	0.06
N4258(−152−037)	0.00	21.4	1.8	0.47	0.04	0.31	0.04
N4258(−032+141)	0.59	75.8	0.5	0.35	0.02	0.02	0.04
N4258(−025+130)	0.58	100.7	1.0	0.33	0.02	0.09	0.04
N4258(−019+121)	1.35	74.4	0.9	0.44	0.02	−0.03	0.05
N4258(−010+110)	0.06	50.9	1.2	0.34	0.02	−0.05	0.05
N4258(−035−086)	1.86	73.6	2.7	0.61	0.02	−0.18	0.07
N4258(+024−170)	0.22	114.5	0.8	0.33	0.02	0.16	0.03
N4258(−005−150)	0.00	169.3	8.8	0.38	0.03	0.16	0.04
N4258(+039−185)	0.00	46.5	4.0	0.49	0.04	0.24	0.04
N4258(−014−038)	0.00	142.6	5.1	0.27	0.03	−0.35	0.11
N4736(+116−038)	0.73	100.4	2.1	0.38	0.02	−0.32	0.09
N4736(+123−055)	0.85	551.9	31.2	0.38	0.03	−0.12	0.07
N4736(+037+009)	0.05	49.0	1.0	0.28	0.03	0.06	0.04
N4736(+037+003)	0.60	251.4	2.4	0.31	0.02	−0.18	0.07
N4736(+032−016)	0.00	18.5	1.4	0.34	0.05	−0.23	0.10
N4736(−029+014)	0.00	225.8	8.5	0.23	0.03	−0.35	0.10
N4736(−036−003)	1.77	54.3	1.5	0.48	0.02	−0.21	0.07
N4736(−038+009)	0.48	47.3	0.7	0.22	0.03	−0.46	0.13
N4736(−039+020)	0.97	71.0	1.0	0.35	0.02	−0.12	0.06
N4826(−006+016)	1.52	31.5	2.1	−0.35	0.11	−1.35	1.16
N4826(−012+019)	1.33	24.1	1.4	−0.41	0.13	−1.16	0.73
N4826(−017+020)	1.58	38.6	2.0	−0.35	0.11	−0.84	0.34
N4826(+008+012)	2.44	46.2	2.7	−0.18	0.08	−0.95	0.45
N4826(+015+011)	1.03	46.2	2.0	−0.40	0.13	−1.02	0.50
N5005(−040−015)	0.00	15.1	1.2	−0.10	0.09	−0.47	0.16
N5701(−007−088)	0.03	153.7	5.9	0.29	0.03	0.23	0.03
N5701(+080−060)	0.00	125.6	4.8	0.32	0.03	0.06	0.04
N5701(−096+040)	0.00	58.2	9.2	0.40	0.08	0.15	0.08
N6384(−002−083)	2.62	61.0	3.7	0.54	0.02	−0.38	0.12
N6384(+004−078)	0.00	36.9	5.5	0.31	0.08	−0.29	0.16
N6384(+024−067)	0.10	40.9	1.4	0.17	0.04	−0.33	0.10
N6384(+051+037)	2.04	46.6	3.9	0.05	0.06	−1.43	1.52
N6384(−032+076)	0.00	55.2	5.4	0.21	0.06	−0.02	0.07
N6384(−033+075)	0.33	59.1	2.9	0.34	0.03	−0.13	0.07
N6384(−041+070)	2.70	68.7	5.6	0.64	0.02	−0.03	0.07
N6384(+130+110)	0.00	62.8	6.4	0.47	0.05	0.40	0.04
N6384(−018+084)	1.49	109.9	7.9	0.34	0.04	−0.05	0.06
N7331(−032−016)	0.00	23.1	1.2	0.31	0.04	−0.14	0.07
N7331(−028+018)	1.36	16.3	1.0	0.17	0.04	−0.45	0.15
N7331(−028+013)	0.00	12.3	1.8	0.28	0.08	−0.21	0.13
N7331(−031+024)	1.66	65.0	3.8	0.32	0.03	−0.20	0.08
N7331(−034+037)	1.76	33.9	2.4	0.40	0.03	−0.35	0.12
N7331(−032+027)	0.39	25.8	1.8	0.17	0.05	−0.65	0.23

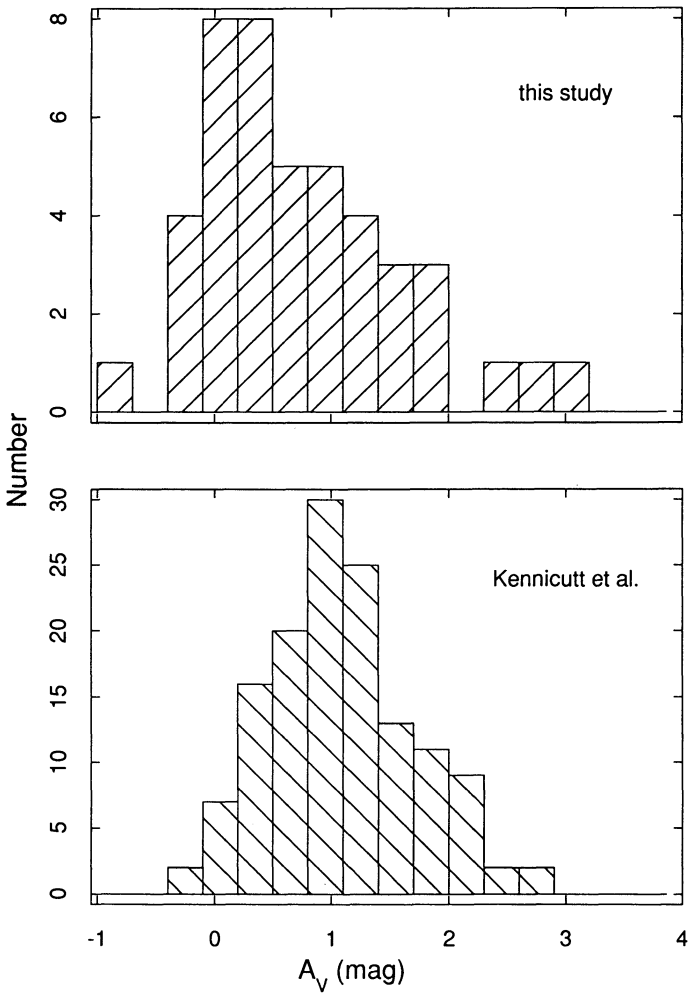

FIG. 2.—Extinctions in our sample of early-type galaxies (*top*) peak at similar values to those previously found in extragalactic H II regions, compiled by Kennicutt et al. (1989, *bottom*).

actually *lower* than for the Kennicutt et al. sample (1.0 mag), despite the fact that our values have not been corrected for Galactic extinction (<0.1 mag for most galaxies). Given the considerable dispersion in the two samples and the lack of Hα-based Balmer decrements in our data, we do not believe the difference is significant. However, the data clearly exclude systematically higher extinction in the H II regions of early-type spirals. While our data do harbor a selection effect favoring the brightest, and perhaps least reddened, objects in our galaxy sample, one would nevertheless expect even these H II regions to be heavily reddened if extinction were responsible for the faintness of the population as a whole. One would furthermore expect such a bias to affect both samples in Figure 2, although it could be somewhat less in the late-type sample. The low luminosities of the H II regions observed in the early-type galaxies must therefore be due to other physical causes, as discussed by Kennicutt, Edgar, & Hodge (1989).

One might naively expect that higher metal abundances in the early-type disks (next section) could be associated with higher dust content and extinction. However, the results in Figure 2 demonstrate that the situation is more complex. The H II regions in the Sa–Sb galaxies are much smaller on average than their counterparts in the bottom panel of Figure 2, and if they are also associated with smaller molecular and atomic clouds, the column density of gas, and presumably dust, along the line of sight might well be lower than in the larger H II regions. We note that H II regions in galaxies with strong radial abundance gradients show weak, if any, gradients in extinction (e.g., van der Hulst et al. 1988; Belley & Roy 1992; Scowen, Dufour, & Hester 1992), which also demonstrates that abundance and extinction are not necessarily correlated.

3.2. *Abundances*

A qualitative indication of the excitation range of our sample is illustrated in Figure 3, which shows the run of [O II]/Hβ against [O III]/Hβ. (Throughout the remainder of the paper we will use "[O II]" and "[O III]" to denote the sum of the flux in the optical doublet of the named ion.) The dashed line shows the mean locus of line ratios for H II regions in the study by MRS, which included galaxies of types Sab–Im, but predominantly consisted of Sbc–Scd galaxies. For most of our H II regions the flux of [O III] < Hβ, placing them on the higher abundance branch of the double-valued excitation sequence, R_{23} (see below). In view of the upper limits and large uncertainties for our low-excitation objects, we do not feel the trend of slightly higher emission in [O III] in comparison to MRS is significant. One object, N1068(+019+010), marked with the arrow in Figure 3, appears to deviate significantly from the correlation. This H II region lies directly in the path of the diffuse, high-excitation "cone" associated with the Seyfert nucleus of NGC 1068 (e.g., Bland-Hawthorn, Sokolowski, & Cecil 1991; Pogge 1988), and it is possible that contamination from this source is responsible for its anomalous excitation properties.

For most of the H II regions in our sample, a direct heavy element abundance determination, based on measurements of the electron temperature and density, cannot be obtained. The [O III] λ4363 auroral line, which is the most commonly applied temperature indicator in extragalactic H II regions, is expected to be of order 10^2–10^3 times fainter than the [O III] λ5007 line, yet in many of our objects even the 5007 Å line is barely, if at all, detected. Consequently we have based our abundance comparison on the "empirical" method of Pagel et al. (1979), in which the abundance is calibrated against $R_{23} \equiv$ ([O II] + [O III])/Hβ. Both the calibration and accuracy of this parameter are uncertain, due to the dearth of observational anchor points at high abundance, and an incomplete understanding of how other physical parameters may affect the excitation. But it is generally agreed that the overall qualitative behavior of these lines is primarily due to changes in chemical abundance (e.g., Dinerstein 1990), as originally shown by Searle (1971). The reliability of the R_{23} method is especially critical for our application, since we are applying it in regimes of abundance and nebular luminosity which in some cases are substantially different from the regime in which the method was calibrated. In this section we use the R_{23} method to estimate abundances for the H II regions and to analyze the characteristics of our sample. We discuss the reliability of these abundances in detail in § 4.

The abundances derived here are based on the (O/H) versus R_{23} calibration of Dopita & Evans (1986). Our choice was based on the comparison of calibrations by McGaugh (1991). There are tentative suggestions that the mean effective temperatures of the ionizing stars in H II regions decrease with increasing metallicity (e.g., Viallefond 1985; Vílchez & Pagel 1988), or that the nebular ionization parameter decreases sys-

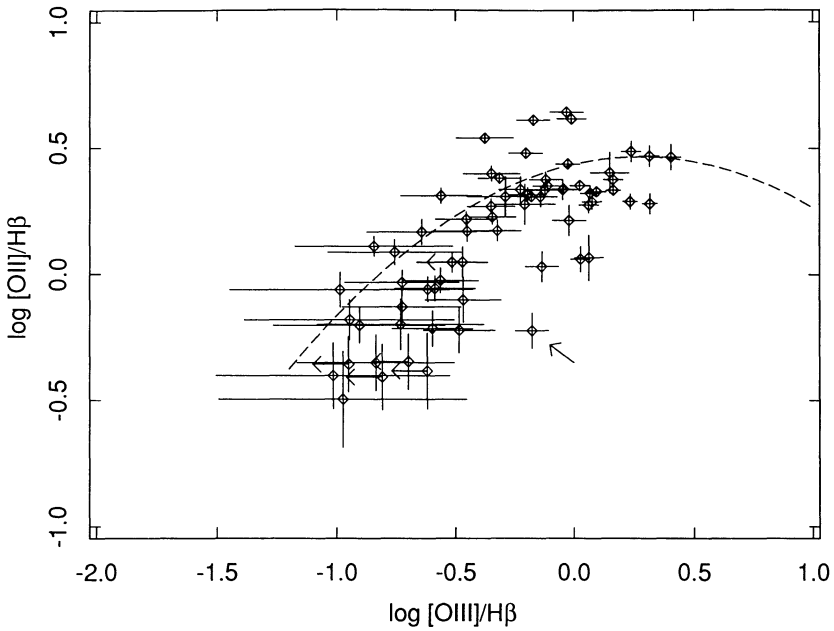

FIG. 3.—Correlation of [O II]/Hβ vs. [O III]/Hβ appears normal compared to that observed by MRS (*dashed line*). The marked object, N1068(+019+010), is a possible exception and may be an unusual object (*see text*).

tematically with increasing abundance (Evans & Dopita 1985). This introduces a flattening of the (O/H) versus R_{23} calibration at high abundance, as can be seen in McGaugh's work. In the particular range of $-0.4 \lesssim R_{23} \lesssim 0.8$ covered by our data, this is precisely the behavior of the Dopita & Evans calibration, which we adopt based on qualitative arguments in light of McGaugh's models, rather than its physical basis. Over the range of R_{23} of interest here, this calibration generally gives somewhat lower abundances than the calibrations of Edmunds & Pagel (1984) or MRS. Adopting the latter calibrations would tend to *increase* the mean abundances in our sample, and increase the difference in abundance between our sample and the late-type galaxy sample of MRS.

The derived abundances for the H II regions in our sample, given as 12 + log (O/H), are listed in Table 3, along with low and high values derived with the errors on the corresponding R_{23}. We also provide the R_{23} measurements themselves, so that readers who wish to convert to a different abundance calibration may do so. The quoted measurement error in this excitation parameter is formally propagated from those of the individual line fluxes and includes the same factors described in the errors for line ratios given in Table 2. For reference, an extreme error of 2 mag in A_V corresponds to an error $\sim$0.2–0.3 in R_{23} and a difference of roughly 0.1 dex in abundance, depending on the excitation. Nevertheless, we emphasize the substantial amount of real scatter that remains in the data. One should also bear in mind that, as discussed in § 4, the intrinsic uncertainty in the R_{23}-derived absolute abundances in this excitation regime is a systematic error of $\sim$0.3 dex.

Table 3 also lists each object's galactocentric radius r, based on the angle of inclination and position angle given in Table 1, assuming $H_0 = 75$ km s^{-1}/Mpc. In addition, we computed the "effective fractional radius" r/R_E, the galactocentric radius normalized to the effective radius R_E from Table 1. These were taken to be simply half the "effective aperture" A_e (half light diameter), given in de Vaucouleurs, de Vaucouleurs, & Corwin (1976, hereafter RC2), except in the cases of NGC 3351 and NGC 4736, whose effective disk radii were given by McCall (1982). For NGC 772, no A_e was available, so its log $2R_E$ was taken to be log D_0 minus the mean (log D_0 − log $2R_E$) of the rest of the sample. Similarly, Table 3 also provides the "isophotal fractional radius" r/R_0, which is the fractional radius normalized to the isophotal radius R_0 from Table 1, also from RC2.

Figure 4 compares the distribution of abundance in our sample with that of MRS, who studied a large sample of H II regions in predominantly late-type galaxies. We have selected for comparison all their objects in galaxies of type Sc and later, using MRS's revised classifications, with the exception of NGC 4254, a Virgo cluster member whose abundance pattern is likely to be affected by the cluster environment (Shields et al. 1991). The remaining comparison sample is composed of 54 H II regions in 12 galaxies, the majority of which are classified as Scd galaxies, although if the RSA classifications were used, the majority would be Sc galaxies.

It is immediately apparent from Figure 4 that the objects in our sample of early-type galaxies (upper panel) show a higher mean abundance than those in the late-type galaxies (lower panel). The mean of our distribution is 12 + log (O/H) = 8.97, a factor of about 1.5 greater in (O/H) than the comparison sample mean of 12 + log (O/H) = 8.77. These correspond to a mean log R_{23} of 0.29 for the early-type galaxies, and 0.61 for the late-types. Also notable in Figure 4 is the absence of objects in our sample with abundances lower than 12 + log (O/H) = 8.71. For reference, Baldwin et al. (1991) quote an abundance for the Orion nebula of 8.58, and Aller (1987) quotes a solar oxygen abundance of 8.91. Note that there is a large, real dispersion in both distributions, which causes a considerable overlap between the two samples. It is important to bear in mind the relative insensitivity of the adopted R_{23} calibration at higher abundance, and that the data in Figure 4 correspond to a dramatic range in mean excitation. The difference in mean abundances on this scale represents a difference of greater than a factor of 2 in R_{23} excitation.

TABLE 3

ABUNDANCES

Object	r (kpc)	r/R_E	r/R_0	log R_{23}	Error	12+ log (O/H)	Abundance −error	Abundance +error
N772(+024+060)	6.09	0.61	0.18	0.16	0.04	9.03	9.02	9.04
N1068(−025−036)	3.59	0.88	0.21	0.05	0.04	9.06	9.05	9.07
N1068(−025−032)	3.30	0.79	0.19	0.05	0.04	9.06	9.05	9.07
N1068(−013−008)	1.22	0.29	0.07	−0.07	0.05	9.09	9.07	9.10
N1068(−032+001)	2.86	0.71	0.17	0.34	0.03	8.98	8.97	8.99
N1068(−021+020)	2.92	0.71	0.17	0.26	0.04	9.00	8.99	9.02
N1068(+019+010)	1.73	0.42	0.10	0.10	0.03	9.05	9.04	9.05
N1068(+023+017)	2.28	0.54	0.13	−0.01	0.06	9.08	9.06	9.09
N1068(−019+009)	2.05	0.50	0.12	−0.03	0.06	9.08	9.06	9.10
N2460(−017+003)	2.34	1.07	0.25	0.36	0.06	8.97	8.95	8.99
N2460(−197−096)	24.47	11.18	2.62	0.60	0.03	8.84	8.82	8.86
N2841(−042+086)	4.44	1.60	0.45	−0.09	0.10	9.09	9.07	9.12
N3031(+107−291)	2.55	1.49	0.44	0.49	0.03	8.91	8.89	8.92
N3351(+023+067)	2.94	1.25	0.33	−0.37	0.16	9.17	9.13	9.21
N3351(+000+068)	2.93	1.25	0.33	−0.30	0.15	9.15	9.11	9.19
N3351(−058−135)	6.16	2.58	0.68	0.08	0.04	9.05	9.04	9.06
N3351(−088−026)	5.24	2.20	0.58	−0.12	0.06	9.10	9.09	9.12
N3351(−105−086)	6.70	2.81	0.74	0.15	0.04	9.03	9.02	9.04
N3351(−001+006)	0.28	0.11	0.03	−0.31	0.11	9.15	9.12	9.18
N3368(+054−024)	3.27	1.00	0.33	0.05	0.04	9.06	9.05	9.07
N3368(+054−026)	3.31	1.00	0.33	−0.03	0.06	9.08	9.06	9.10
N3368(−052+025)	3.19	0.97	0.32	0.37	0.03	8.97	8.96	8.98
N3623(−003−086)	4.37	1.39	0.41	0.15	0.05	9.03	9.02	9.05
N4258(−318+183)	20.31	3.58	1.27	0.71	0.02	8.74	8.72	8.77
N4258(−152−037)	14.20	2.51	0.89	0.70	0.04	8.75	8.72	8.79
N4258(−032+141)	6.15	1.07	0.38	0.52	0.01	8.90	8.89	8.90
N4259(−025+130)	5.85	1.04	0.37	0.53	0.01	8.89	8.88	8.90
N4258(−019+121)	5.64	0.99	0.35	0.57	0.01	8.86	8.86	8.87
N4258(−010+110)	5.47	0.96	0.34	0.49	0.02	8.91	8.90	8.92
N4258(−035−086)	7.13	1.27	0.45	0.68	0.02	8.77	8.76	8.79
N4258(+024−170)	8.05	1.41	0.50	0.56	0.01	8.87	8.86	8.88
N4258(−005−150)	8.59	1.52	0.54	0.58	0.03	8.85	8.83	8.87
N4258(+039−185)	8.18	1.44	0.51	0.68	0.04	8.77	8.73	8.80
N4258(−014−038)	3.03	0.54	0.19	0.36	0.03	8.97	8.96	8.98
N4736(+116−038)	2.77	2.09	0.38	0.46	0.02	8.93	8.92	8.94
N4736(+123−055)	3.02	2.25	0.41	0.50	0.03	8.91	8.89	8.92
N4736(+037+009)	0.95	0.71	0.13	0.48	0.02	8.92	8.91	8.93
N4736(+037+003)	0.90	0.66	0.12	0.43	0.02	8.94	8.93	8.95
N4736(+032−016)	0.80	0.60	0.11	0.44	0.04	8.94	8.92	8.96
N4736(−029+014)	0.72	0.55	0.10	0.33	0.03	8.98	8.97	8.99
N4736(−036−003)	0.87	0.66	0.12	0.56	0.02	8.87	8.86	8.88
N4736(−038+009)	0.89	0.66	0.12	0.30	0.02	8.99	8.98	9.00
N4736(−039+020)	0.98	0.71	0.13	0.48	0.02	8.92	8.91	8.93
N4826(−006+016)	0.59	0.36	0.10	−0.31	0.12	9.15	9.12	9.18
N4826(−012+019)	0.66	0.40	0.11	−0.34	0.13	9.16	9.13	9.19
N4826(−017+020)	0.71	0.44	0.12	−0.23	0.09	9.13	9.11	9.16
N4826(+008+012)	0.59	0.36	0.10	−0.11	0.07	9.10	9.08	9.12
N4826(+015+011)	0.71	0.44	0.12	−0.31	0.11	9.15	9.12	9.18
N5005(−040−015)	6.09	2.13	0.63	0.05	0.07	9.06	9.04	9.08
N5701(−007−088)	8.50	1.95	0.63	0.56	0.02	8.87	8.85	8.88
N5701(+080−060)	9.36	2.13	0.69	0.51	0.02	8.90	8.89	8.91
N5701(−096+040)	9.66	2.19	0.71	0.59	0.07	8.84	8.79	8.89
N6384(−002−083)	10.66	1.26	0.49	0.59	0.02	8.85	8.83	8.86
N6384(+004−078)	10.32	1.21	0.47	0.41	0.08	8.95	8.92	8.98
N6384(+024−067)	10.46	1.23	0.48	0.29	0.03	8.99	8.98	9.00
N6384(+051+037)	7.52	0.90	0.35	0.06	0.07	9.05	9.04	9.07
N6384(−032+076)	12.18	1.44	0.56	0.41	0.05	8.95	8.93	8.97
N6384(−033+075)	12.15	1.44	0.56	0.46	0.03	8.93	8.91	8.94
N6384(−041+070)	12.42	1.47	0.57	0.73	0.02	8.73	8.70	8.75
N6384(+130+110)	19.90	2.36	0.92	0.74	0.04	8.72	8.67	8.76
N6384(−018+084)	12.02	1.41	0.55	0.49	0.03	8.91	8.90	8.93
N7331(−032−016)	7.62	1.65	0.37	0.44	0.03	8.94	8.92	8.95
N7331(−028+018)	5.70	1.25	0.28	0.26	0.04	9.00	8.99	9.01
N7331(−028+013)	5.74	1.25	0.28	0.40	0.07	8.96	8.92	8.98
N7331(−031+024)	6.20	1.34	0.30	0.43	0.03	8.94	8.93	8.95
N7331(−034+037)	6.66	1.43	0.32	0.47	0.03	8.92	8.91	8.94
N7331(−032+027)	6.37	1.38	0.31	0.23	0.05	9.01	9.00	9.02

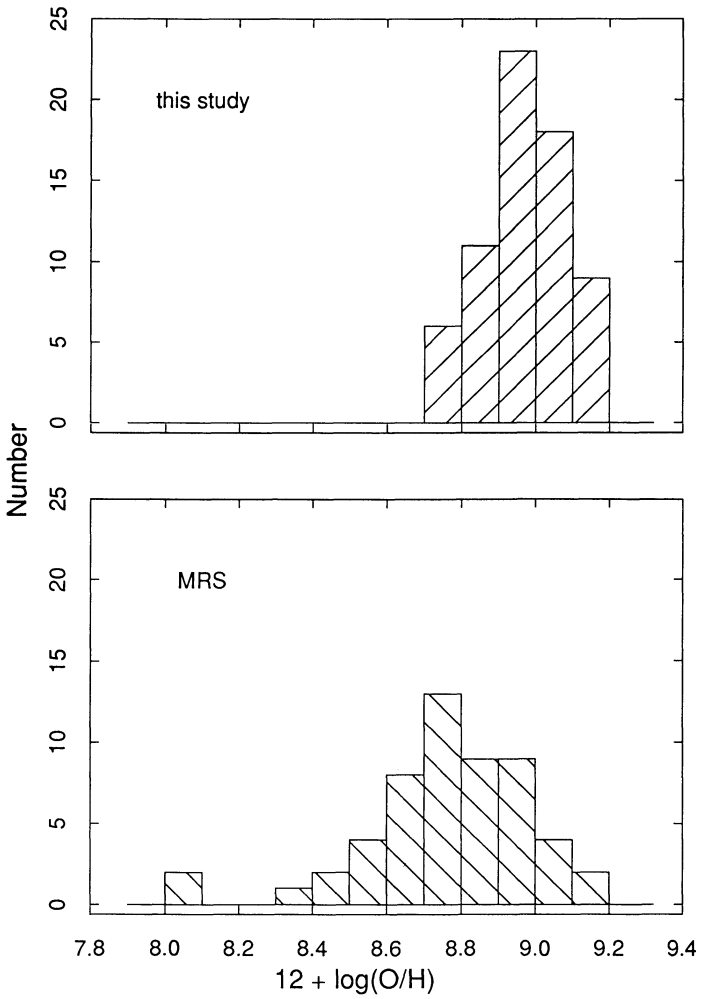

FIG. 4.—Abundances in early-type galaxies (*top*) are systematically higher than in the comparison sample, which consists of the Sc and later-type galaxies from MRS (*bottom*).

An important factor which affects the interpretation of the abundance distributions in Figure 4 is the well-known radial metallicity gradient in spiral galaxies (e.g., Searle 1971; Pi-embert 1975; Shields & Searle (1978). Figure 5 presents the H II region abundances as a function of their effective fractional radii (Table 3). Note that the error bars represent measurement errors only and do not include systematic uncertainties in the calibration of R_{23} as mentioned above. In some of the galaxies the H II regions do not cover a sufficient radial extent to test for a gradient, but those that have good radial sampling show decreasing abundances with radius. We confirm the findings by Evans & Dopita (1987), that the Seyfert 2 galaxy NGC 1068 exhibits normal abundances, and it also exhibits a metallicity gradient. We also caution that the outlying object N2460(−197−096) may be associated with the nearby H II galaxy IC 2209, or may be a tidally induced knot of star formation. However, this H II region does appear to fall along an outer arm of NGC 2460, so we tentatively include it in our sample.

Figure 6 compares the abundance distributions in early- and late-type galaxies. It is again apparent that the increase in mean abundance for the early-type galaxies is not due to selection effects favoring objects at smaller radii; Figure 6 shows that the net abundance is higher at all fractional radii. But again, there is considerable overlap between the two samples, and some late-type galaxies such as M51 (Díaz et al. 1991) or M83 (Dufour et al. 1980) possess H II regions as metal-rich as any in our galaxy sample. The main difference in the early-type sample rather appears to be a lack of low abundance objects. From this, it is reasonable to expect that the galaxies with higher overall metallicities should show shallower abundance gradients, since these gradients appear to be "normalized" at similar peak abundances near the galactic centers. This is somewhat suggested by the data in Figure 6.

Indeed, the abundance gradients in these early-type galaxies do suggest a trend of slightly shallower gradients than those found in late-type systems. Using the parameterization of Díaz (1989):

$$(\mathrm{O/H})_r = (\mathrm{O/H})_{R_E} \times 10^{-a_E(r/R_E-1)}, \quad (1)$$

we find a median a_E of 0.08 by a simple, single-line fit. On the other hand, the median a_E for the MRS subsample is 0.29. This fairly dramatic difference is shown in Figure 6*a*, where the fitted gradients for the various galaxies are overplotted on the data. The values of a_E for our data are given in Table 4. We note that the measured gradients are somewhat dependent on the abundance calibration employed, and that a steeper calibration would lead to slightly steeper gradients. We have also verified that the gradients of the late-type galaxies are not due solely to the outlying low-metallicity objects, whose abundances are much more sensitive to the calibration.

The difference in gradients between the two samples is probably not as significant as first appears, when one considers that the measurement of R_E is substantially affected by the galactic bulge at earlier Hubble types. This is demonstrated in Figure 6*b*, where we plot the gradients based on the isophotal fractional radii, a_0, also listed in Table 4. The trend of shallower gradients is still present, with a median a_0 of 0.28 for the early-type galaxies, versus 0.44 for late-type, but the difference is much less pronounced. Note especially the relative change in the fractional radii of objects in early- and late-type galaxies between Figures 6*a* and 6*b*. Since neither of these methods provides a suitable radial normalization for the H II regions, any trend of gradient slope with Hubble type remains far from established, but it is suggestive that the sense of the trend is consistent between both normalizations. Ideally the normalization should be to an R_E of the disk only, which we were able to obtain only for NGC 3351 and NGC 4736 (McCall 1982). Clearly, Figure 6 demonstrates the importance of the choice of radial normalization employed.

A second factor which may affect our abundance comparison between early- and late-type galaxies is a correlation suggested by Garnett & Shields (1987), that the mean abundance of spiral disks may be more strongly tied to galaxy luminosity and mass, rather than morphological type. Figure 7 shows the relation of H II region excitation with the integrated luminosity, M_B^0 from Table 1, of the parent galaxy for the objects in our sample (solid points), and the MRS sample (open points). Here the abundance parameter R_{23} is plotted for each H II region, thus each vertical set of points represents a single galaxy. This comparison of excitation as function of galaxy luminosity, rather than mass, avoids possible inconsistencies between different authors in measuring total masses.

In fact, it is clear from Figure 7 that our sample does consist of galaxies with systematically higher luminosities than the MRS comparison sample, and this is probably responsible for

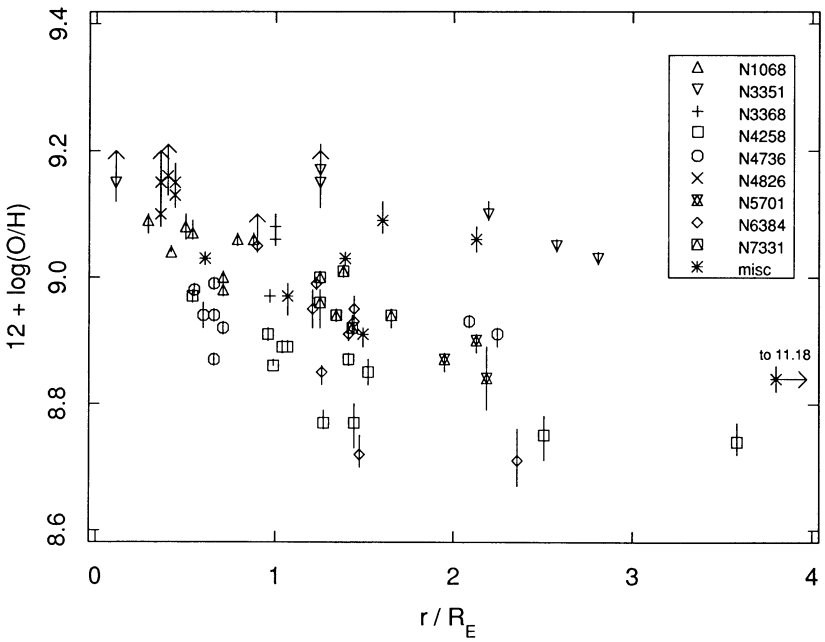

FIG. 5.—Abundances vs. effective fractional radius. Note that the error bars represent measurement errors only and do not include the uncertainty in absolute abundance calibration. N2460(−197−096) is actually located at $r/R_E = 11.18$ (*see text*).

at least part of the difference in abundance seen in Figure 4. To test whether this difference is entirely the manifestation of a luminosity-excitation correlation, we attempted a crude correction to the observations. We computed a simple least-squares fit to the data in Figure 7, and then divided this fit into the data, thereby eliminating that correlation. These corrected excitations are replotted in Figure 8*b* as a function of galaxy type, with the same notation as Figure 7. The original data are presented in Figure 8a for comparison, where the abundance-type dependence is readily apparent. While the relative difference in excitation between the early- and late-type galaxies does decrease between Figures 8*a* and 8*b*, it is nevertheless still present; the corrected excitation parameters for the early-type galaxies exhibit a mean of 0.82, while the late-type mean is 1.24. In any case, the systematic change with type (or luminosity) is small compared to the large dispersion in mean abundance among galaxies of the same type.

We replot Garnett & Shields' mass-metallicity relation in Figure 9, adding the abundances of our sample. The characteristic galaxy abundance plotted in this diagram is the mean abundance at R_E. These mean abundances are provided in Table 4, along with the galaxy masses and references. Three methods were used to derive the mean abundances. A few galaxies had actual data points measured near R_E, in which case these points were averaged and the result adopted as the characteristic abundance; this direct method is denoted by a "D" in column (3) of Table 4. In other galaxies where it was possible to fit a gradient, the abundance at R_E was interpolated; this method is denoted by "F" in Table 4. Lastly, "E" for the remaining galaxies indicates an extrapolation from the scanty data, assuming the sample median a_E of 0.08 in the parameterization of equation (1).

The main effect of adding our data (open polygons) to Figure 9 is to increase the number of measurements among

TABLE 4

CHARACTERISTIC ABUNDANCES

NGC (1)	12+ log (O/H) (2)	Method (3)	a_E (4)	a_0 (5)	log $(M/M_\odot)$ (6)	Mass Reference (7)
772.....	9.00	E	...	...	11.9	Fisher & Tully 1981 (FT)
1068.....	9.01	F	0.08	0.38	11.4	FT
2460.....	8.97	D	...	...	11.1	Peterson 1979
2841.....	9.14	E	...	...	11.5	FT
3351.....	9.14	F	0.05	0.19	10.7	Huchtmeier & Seiradakis 1985
3368.....	9.04	D	...	...	11.3	FT
3623.....	9.06	E	...	...	11.3	FT
4258.....	8.89	D	0.07	0.19	11.3	FT
4736.....	8.93	F	0.01	0.07	10.5	Huchtmeier & Seiradakis 1985
4826.....	9.09	E	...	...	10.8	FT
5005.....	9.14	E	...	...	11.4	Helou et al. 1982
5701.....	8.95	E	...	...	10.9	Huchtmeier 1982
6384.....	8.99	F	0.23	0.55	11.5	Shostak 1978
7331.....	9.00	F	0.11	0.46	11.7	FT

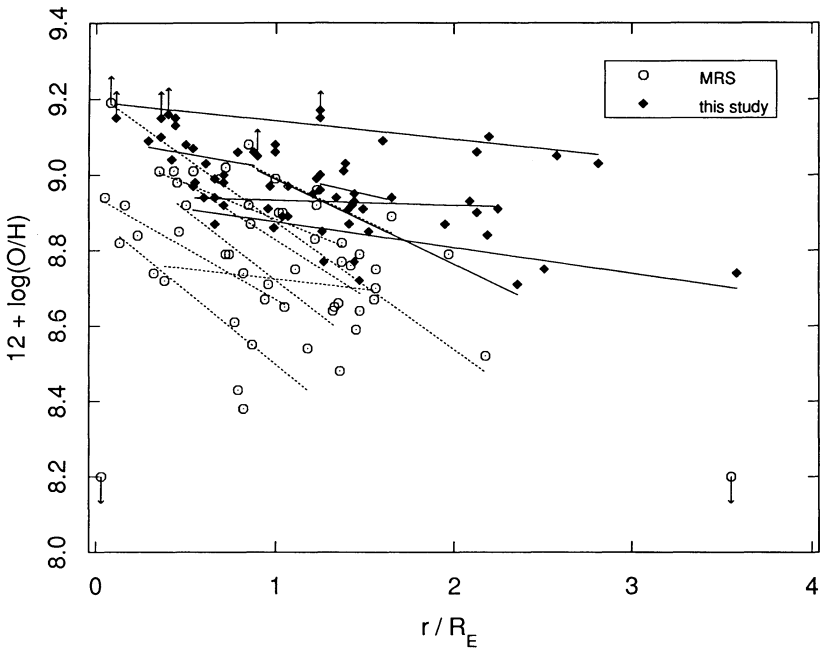

FIG. 6a

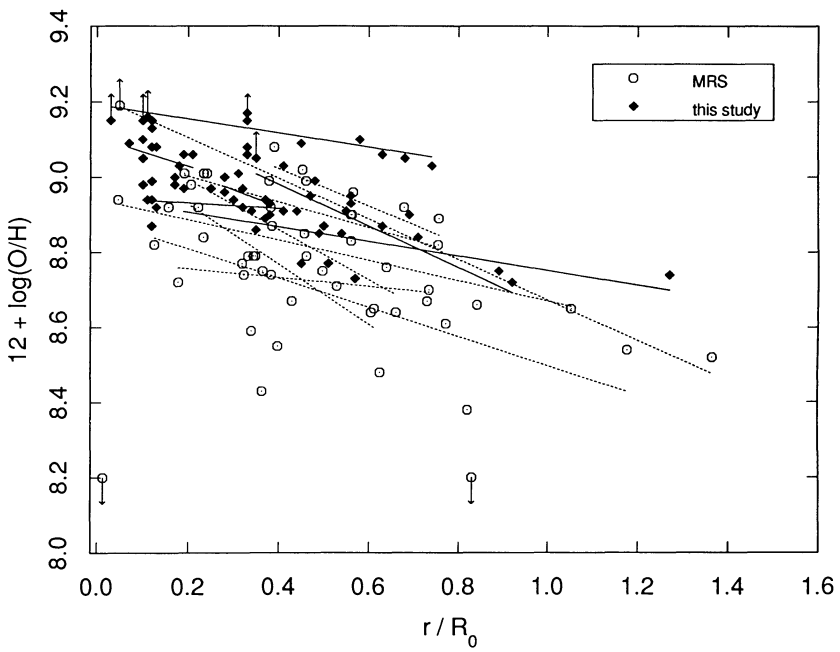

FIG. 6b

FIG. 6.—Abundances of early-type galaxies (*solid points*) are higher across all galactocentric radii in comparison to those of late-type galaxies (*open points*). Gradients of early-type galaxies (*solid lines*) also tend to be systematically flatter compared to those of late-type (*dotted lines*). This effect is more pronounced when galactocentric radii are normalized to R_E (panel *a*), than when normalized to R_0 (panel *b*) (*see text*).

luminous spirals. At low galaxy masses (10^8–10^{11} $M_\odot$) the abundance-mass correlation is readily apparent. Over that mass range, the sample includes both spiral and irregular galaxies, and the correlation is similar to the abundance-mass relation observed among irregular galaxies alone (e.g., Skillman et al. 1988). However, the spiral galaxies in our sample do not extend this trend to higher masses. It can also be seen that the Sab galaxy M81 (solid point), studied by Garnett & Shields, is typical among its spiral cohorts on the diagram. The distinctive absence of the mass-metallicity correlation in our sample is rather puzzling and is suggestive that other parameters (e.g., morphological type, gas content, disk surface density) may also be coupled to the chemical abundances of the disks. Further study is needed to isolate the effects of each parameter, and a more detailed investigation of this problem is currently in progress (Zaritsky, Kennicutt, & Huchra 1993).

Most authors have discussed the changes in abundance with galaxy radius and morphological type in terms of chemical

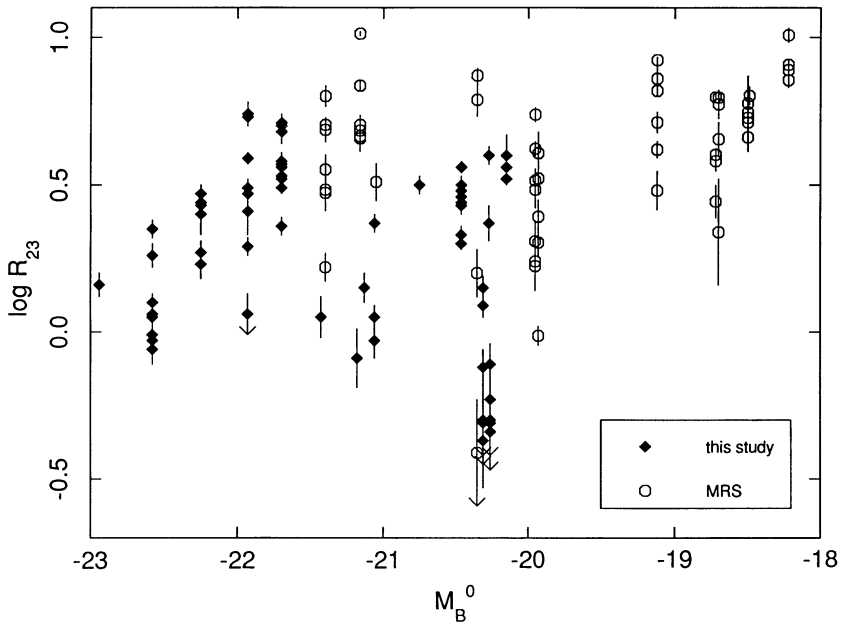

FIG. 7.—Correlation of the observed abundance parameter R_{23} vs. absolute blue magnitude of the host galaxies, with the early-type sample shown in solid symbols, and late-type sample in open symbols.

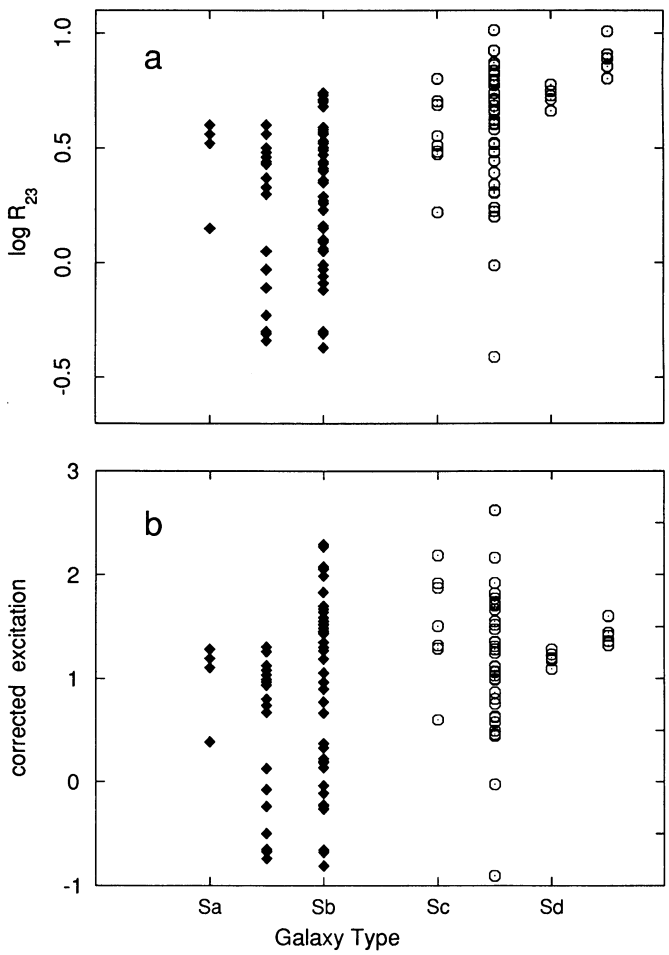

FIG. 8.—Observed H II region excitations (using the same notation as Fig. 7) exhibit a correlation with galaxy type. Panel (*a*) shows the observed R_{23} vs. galaxy type, while panel (*b*) shows the relative excitations corrected for the luminosity-excitation correlation. For clarity the upper limits are not indicated.

evolution. Within the framework of the simple closed box evolution model, the abundances of oxygen and other primary heavy elements would be expected to increase as the disk gas fraction decreases. Qualitatively, our results can be understood if the early-type galaxies have lower gas fractions than their late-type counterparts. Unfortunately there is very little published data on spatially resolved gas distributions in these galaxies, so we cannot perform a quantitative test of this model. (Unresolved data will not suffice since such observations are usually dominated by the vast tracts of atomic gas beyond the star-forming disks.) We note that there are a number of physical mechanisms, such as star formation thresholds (Kennicutt 1989), or inflows (Lacey & Fall 1985) that would tend to impose an upper limit on gas-phase metallicity in luminous, gas-poor systems. An example of a chemical evolution model that appears to fit our data is that of Galli & Ferrini (1989). These authors attempt to address the changes in star formation properties along the Hubble sequence by coupling halo and disk components via infall from the former to the latter. Mollá et al. (1992) are developing a follow-up model which employs a decreasing infall rate to address the evolution of abundance gradients. This model predicts a flattening of the gradients as a saturation limit is reached at progressively larger galactocentric radii. Our observed abundances and gradients are in reasonable agreement with the predictions of these models. A more detailed analysis regarding galaxy evolution is beyond the scope of this paper and will be addressed when more comprehensive data are available.

4. MODELING OF R_{23} AT HIGH ABUNDANCE

As mentioned earlier, there is no direct calibration of the R_{23} abundance parameter in the low-excitation regime of interest here, and it is therefore important to evaluate the reliability of the method under these conditions. Stasińska (1990) and Díaz et al. (1991) have published photoionization models of metal-rich H II regions and have found that the behavior of the diagnostic [O II] and [O III] lines can be sensitive to variations in parameters other than abundance alone. Since the conclu-

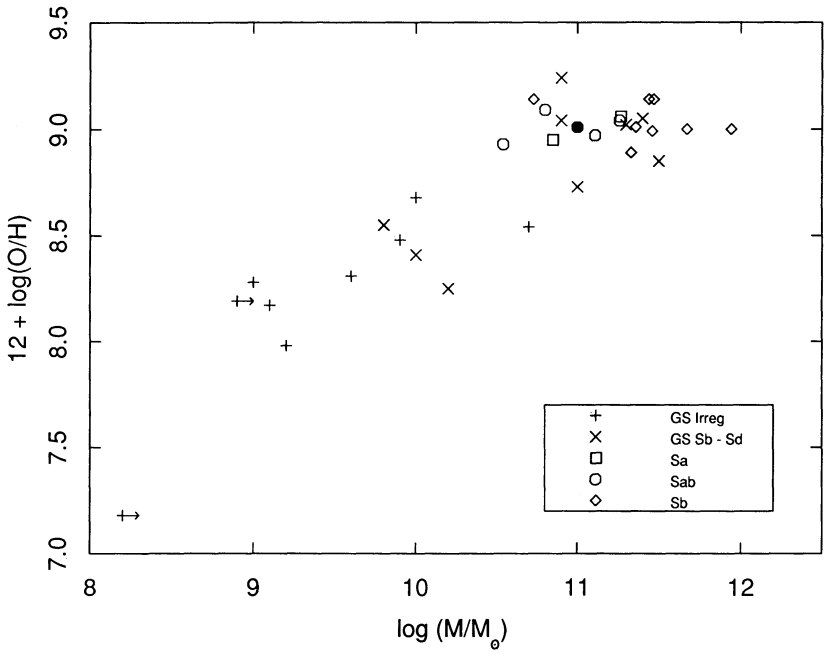

FIG. 9.—Mass-metallicity correlation from Garnett & Shields (1987, GS), incorporating our early-type galaxies shown by the polygons. The spiral galaxies, including those from both papers, do not exhibit a strong mass-metallicity correlation. M81 from GS (shown in black) falls among the bulk of the spirals.

sions of the previous section depend critically on the use of R_{23} as at least a qualitative abundance indicator, we have run a more complete set of photoionization models, covering a wider range of physical conditions in the H II regions.

In order to interpret the behavior of R_{23} at these high abundances, it is important to follow the energy balance in the oxygen lines, as this element provides the dominant cooling in H II regions in most metallicity ranges of interest (e.g., Shields 1990; Dinerstein 1990). Below solar metallicity, the optical lines of O^{++} and O^{+} contribute substantially to the radiative emission. However, at higher abundances the overall cooling rate increases, dominated by the far-infrared fine-structure lines of the O^{++} ground state. Infrared lines from N^{++}, S^{++}, Ne^{+}, and lower-ionization species also contribute to lower the nebular temperatures, which in turn suppresses collisional excitations of the optical forbidden lines. The combined effect of the increased abundance is thus an increase in the fluxes of the fine-structure lines, while the optical transitions show weakening emission.

To explore the behavior of R_{23} in the high-metallicity regime, we calculated photoionization models for H II regions with a range of abundances, ionizing spectra, densities, and ionization parameters, using a program kindly provided by G. Shields. This is an updated version of the code used to analyze H II region spectra in, for example, Shields & Searle (1978) and MRS. Models were made at 0.5, 1, 2, and 3 $Z_\odot$, and with the two different stellar ionizing temperatures of 45,000 and 38,000 K. The solar abundances adopted were those of Aller (1987). The stellar fluxes were estimated as described in Shields & Searle (1978), based on the stellar atmospheres of Hummer & Mihalas (1970a, b). These model atmospheres provide sufficiently similar results to the Kurucz (1979) models (Evans 1991) for the purposes of this simple investigation. The diffuse nebular radiation field was treated in the on-the-spot (OTS) approximation for $T_* = 45{,}000$ K, and in the outward-only approximation for the $T_* = 38{,}000$ K models, since for most 38,000 K models the O^{++} zone is small enough that an outward-only treatment gives a better approximation of the [O III] lines (MRS). In such cases OTS overestimates the ionization rate in the [O III] zone from the softer diffuse radiation field and leads to anomalously low electron temperatures and emission in the [O III] zone. The effects of dust were not incorporated into any of our models. Since the H II regions in our sample do not exhibit anomalously high extinctions (§ 3.1), this should not be a significant problem.

It is conventional to parameterize the model grids in terms of the nebular ionization parameter U:

$$U \equiv \frac{Q(\mathrm{H}^0)}{4\pi R_S^2 nc}, \tag{2}$$

where $Q(H^0)$ is the photon luminosity shortward of the Lyman limit, R_S is the radius of the Strömgren sphere, n is the hydrogen number density, and c is the speed of light. Alternatively, U may also be expressed as being dependent only on the combination of three parameters, $(nf^2Q)^{1/3}$ (e.g., MRS), where f is the nebular filling factor. Since U is effectively proportional to the density of ionizing photons divided by that of electrons in the nebula, models with the same abundance and constant U generate similar ionization structures and similar optical spectra, independent of n, Q, or f, if there are no other factors affecting the behavior of the three parameters. As we will see below, this simple behavior breaks down at high abundance, and the interpretation of the optical spectra becomes more complicated.

The results of our models are shown in Figures 10 and 11. Each set of tracks represents a series of models computed for a particular abundance and stellar temperature. Abundance is indicated by the line type (four values), while stellar temperature is indicated by the symbol size (large for 45,000 K, small for 38,000 K). Each intersecting set contains three tracks, which are model sequences in which a single parameter (U, n,

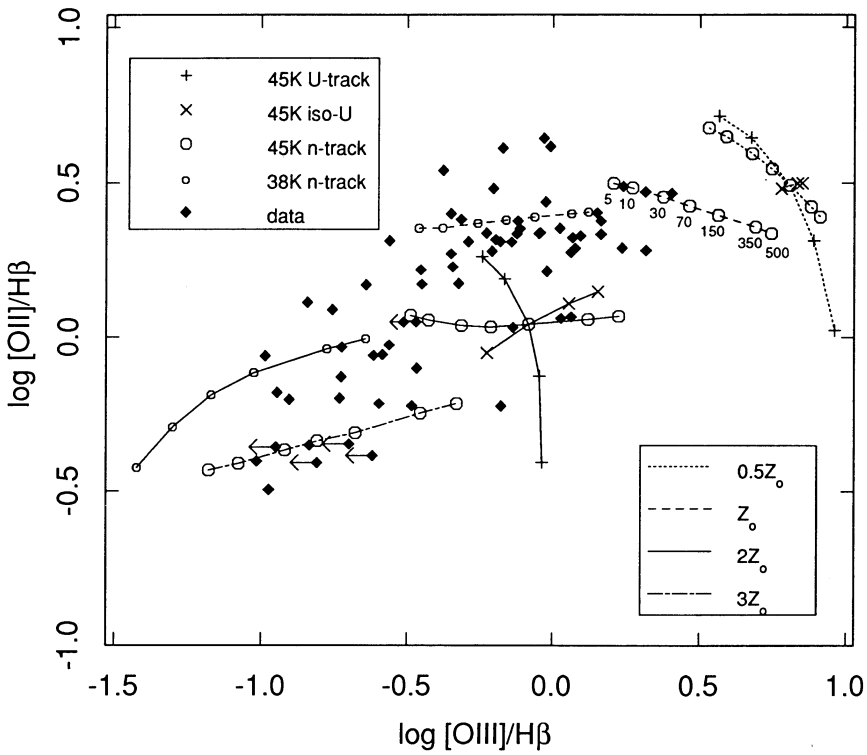

FIG. 10.—Series of one-parameter models superposed on the data. The labels on the $Z_\odot$, 45,000 K n-track show the values of n (cm^{-3}) used for all n-tracks. See text for a detailed description of the symbols.

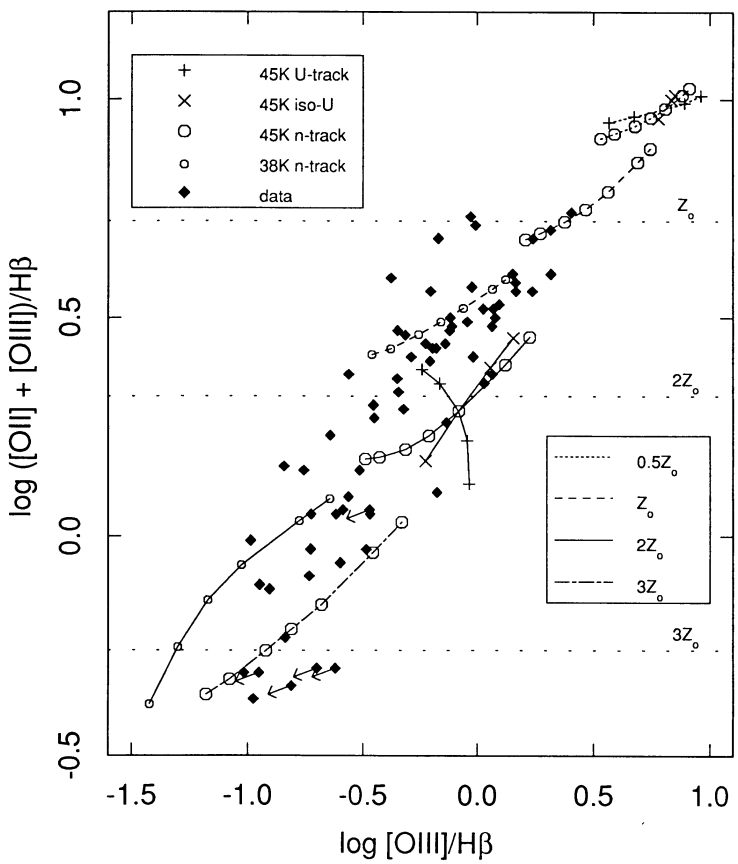

FIG. 11.—Effect of varying parameters on R_{23} (*see text*). The horizontal, dotted lines indicate the values of R_{23} corresponding to $Z_\odot$, $2\,Z_\odot$, and $3\,Z_\odot$ in the Dopita & Evans (1986) abundance calibration. Symbols are the same as for Figure 10.

or f) is addressed. Tracks defined by plus signs (+) represent models of changing U, which are identical in every respect except that the filling factor f was varied from 0.005 to 0.300 (decreasing [O II]/Hβ with increasing U). Perpendicular tracks denoted by the cross symbols (×) are models with constant U, which were generated by changing the density n as $1/(f)^{1/2}$. In both tracks, n ranged from 50 at the low-excitation end to 450 cm^{-3}, and f from 0.052 to 0.017. The third set of tracks, denoted by circles, represent models in which only the density n was varied, from 5 to 500 cm^{-3} (increasing excitation with increasing n). The fiducial reference model, where the tracks cross, is for $n = 150$ cm^{-3}, and $f = 0.030$, values typical for giant H II regions (e.g., Kennicutt 1984, MRS). The ionizing luminosity at the ionization threshold of hydrogen was taken to be 1.4×10^{25} ergs s^{-1} Hz^{-1}, corresponding to log $Q(H^0) = 51.2$, and 50.7 for $T_* = 45{,}000$ and 38,000 K, respectively. These are the equivalent of roughly 36 O5 V stars and 49 O7 V stars (Leitherer 1990). Finally, the observed spectra of the H II regions in our sample are indicated by solid symbols.

We discuss each track in Figure 10 individually. This figure plots the principal diagnostic line ratios, [O II]/Hβ versus [O III]/Hβ. As expected, increasing the abundance from 0.5 to 3 $Z_\odot$, while keeping other parameters constant, lowers both line ratios, since the main effect of the abundance increase is a lowering of the nebular electron temperature. Tracks of changing ionization parameter ("U-tracks"), on the other hand, are roughly orthogonal to the abundance dependence, reflecting the changes in the ionization balance, rather than the thermal balance of the nebula.

Perhaps the most surprising result in Figure 10 is the behavior of the tracks with constant ionization parameter (cross symbols). At an abundance of 0.5 $Z_\odot$ the "iso-U" tracks are nearly degenerate, reflecting the textbook statement that H II regions with different densities and filling factors but the same ionization parameters produce nearly identical spectra. At higher abundances, however, this degeneracy breaks down, and models with the same abundance and ionization parameter show very different excitations. Examination of our models shows that this is primarily due to a strong dependence of the thermal equilibrium on the density of the H II region, independent of the ionization parameter. This is shown explicitly by the "n-tracks" of variable density in Figure 10 (circles). The deviation of the n-track from the U-track grows from near-coincidence at 0.5 $Z_\odot$ to approaching perpendicular at 2 $Z_\odot$, clearly emphasizing the presence of an effect invoked by density, besides variation in U. A similar density effect may be seen in the metal-rich models by Stasińska (1990) and Díaz et al. (1991).

We suspect that the density dependence observed in the high-abundance models is due to the competition between radiative and collisional de-excitation of the O^{++} fine-structure lines. The importance of this effect has been recognized for some time (e.g., Stasińska (1990), but not fully explored, so we discuss the mechanism in some detail here. The fine-structure transitions are more susceptible than the optical lines to the effects of collisional de-excitation, since their critical densities are much lower. For $T = 10^4$ K, the critical densities for the $^3P_2$ and $^3P_1$ levels are 4×10^3 and 2×10^3 cm^{-3} respectively, two orders of magnitude less than for the optical $^1D_2$ doublet at $n_c = 7 \times 10^5$ cm^{-3} (Osterbrock 1989). We tested for this effect by setting the transition probabilities for the [O III] fine-structure lines to high values, thereby artificially forcing the de-excitation to take place radiatively. Indeed, at twice solar metallicity, the extreme points of the "iso-U" track closed to within one-third the difference of their original values in [O III]/Hβ, similar to the difference in the extremes at half solar metallicity. This therefore confirms the action of collisional de-excitation in the physical models.

Although densities of giant H II regions are typically of order 100 cm^{-3} (Kennicutt 1984; O'Dell & Castañeda 1984), collisional effects can nevertheless become noticeable. A roughly fixed amount of energy is allotted to collisional de-excitation, since on average each of the thermal electrons must lose of order 10 eV before their energies are low enough to recombine efficiently (G. Shields 1992, private communication). In low abundance H II regions, where optical lines provide much of the radiative cooling, the collisional effects are relatively unimportant. At high abundances, however, where the fine-structure lines are the predominant coolants, the effect does become significant. At high density, the importance of collisional de-excitation maintains high equilibrium temperatures, whereas at low density radiative de-excitation and cooling are efficient, lowering the electron temperature and consequently the strengths of the optical forbidden lines.

We also briefly investigated the effect of differing metallicities between the ionizing stellar atmospheres and ambient gas. Such a situation might be rather unlikely, but is a question of relevant interest. For a stellar radiation field of 45,000 K, increasing the stellar metallicity to twice solar compared to a surrounding H II region of 0.5 $Z_\odot$ increases the O^+ ionization while decreasing that of the O^{++} region by almost the same factor, since the effects of line blanketing soften the ionizing spectrum. Thus the effect on log R_{23} is a decrease of only ~3%, or 0.02 dex, although the observed change in either log [O II]/Hβ or log [O III]/Hβ alone is in the range of 10%. A similar decrease in stellar metallicity for a 2 $Z_\odot$ H II region yields the same conclusions. The effect is more pronounced for a stellar effective temperature of 38,000 K, where a smaller difference of varying the stellar metallicity to twice solar in a $Z_\odot$ nebula yields a change in log R_{23} of 0.02 dex from matched abundances. The inverse situation, with a solar stellar abundance in a 2 $Z_\odot$ nebula, yields an even larger change of 0.06 dex. The sensitivity of this phenomenon at lower T_* has been attributed by Evans (1991) to the fact that the ionization balance between O^+ and O^{++} is sensitive to T_* at lower effective temperatures, but less so at higher temperatures, where O^{++} dominates. However, the overall effect on R_{23} due to differing stellar abundance is still relatively small.

The results of this analysis indicate that at high abundance, density is another factor besides T_* and U that introduces uncertainty and dispersion to the R_{23} abundance scale. This is shown explicitly in Figure 11, which shows the model dependence of log R_{23} itself, with the same notation as in Figure 10. In addition, we have indicated by horizontal, dotted lines the values of R_{23} corresponding the $Z_\odot$, 2 $Z_\odot$, and 3 $Z_\odot$ in the Dopita & Evans (1986) calibration used earlier in this paper. Differences in n between 10 and 200 cm^{-3}, a reasonable range of densities for giant H II regions (Kennicutt 1984; O'Dell & Castañeda 1984), represent a change of almost 0.2 dex in R_{23} at $Z_\odot$, and as much as 0.5 dex for higher abundances. Variations in the stellar ionizing spectrum also remain an additional large uncertainty; indeed, it is almost impossible to distinguish, using R_{23} alone, between an H II region ionized by a 45,000 K radiation field at 2 $Z_\odot$ and one ionized by $T_* = 38{,}000$ K at solar abundance.

Applying these considerations to the low-excitation H II

regions in our sample, it is clear that the absolute abundances estimated from R_{23} in § 3.2 are subject to substantial uncertainties from variations in density and ionizing spectrum, and that the abundance scale itself may be inaccurate. Consequently we cannot establish with certainty whether the lowest excitation H II regions in our sample are 2, 3, or 5 $Z_\odot$ without more information on their densities and stellar contents. On the other hand, the *relative* scale of abundance versus excitation remains intact, and we can be confident that the objects with lowest excitation are significantly more metal-rich than the high-excitation objects. It can be seen from Figures 10 and 11 that abundances of much less than 2 $Z_\odot$ are very unlikely for the low-excitation H II regions; one cannot reconcile the very low R_{23} of those objects with lower metallicities unless unrealistically low densities and stellar temperatures are assumed. It is also unlikely that the low values of R_{23} we observe in the Sa–Sb H II regions are due to the smaller ionizing fluxes of those objects as the effect on U is too small, and if anything would tend to raise R_{23}.

Observations which would constrain the nebular parameters would be helpful, for example, measurements of n from the [O II] ratio $\lambda3726/\lambda3729$ or [S II] $\lambda6717/\lambda6731$, and measurements of the radiation softness parameter $\eta = (O^+/O^{++})(S^{++}/S^+)$ (Vílchez & Pagel 1988), which would give substantial insight on T_*. If T_* decreases systematically with increasing abundance, as has been suggested by several authors (e.g., Shields & Tinsley 1976; Viallefond 1985; Vílchez & Pagel 1988), then it will systematically affect the abundance scale derived for the low-excitation objects. A program of spectrophotometry of these H II regions in the 4700–10,000 Å range is currently underway, and we defer further analysis of this topic to a future paper.

5. CONCLUSIONS

The results of our study show that the abundances in early-type spiral galaxies show a large intrinsic dispersion and tend to have higher metallicities than in galaxies of later morphological type. An investigation of their gas contents would reveal whether this is consistent with simple chemical evolution theory. The abundances we derive do not enhance the mass-metallicity relation observed in spiral and irregular galaxies, and a larger sample of galaxies is needed to clarify the relative importances of galaxy type and mass on disk chemical properties.

We also find that the effects of dust are unimportant in explaining the lower luminosities of H II regions in the early-type galaxies. Their observed faintness must be due to other factors, such as changes in the size of the ionizing associations, or changes in the IMF (Kennicutt et al. 1989). A follow-up program of spectrophotometry, designed to extend the spectral coverage of the H II regions to 10,000 Å has been undertaken in an effort to shed light on this issue.

Those early-type galaxies in our sample which have H II regions over a large range of galactocentric radius exhibit slightly shallower abundance gradients than published samples of late-type spirals. The significance of this result is not strong, however, and more data are needed to confirm it. There is considerable dispersion in the magnitudes of the abundance gradients, regardless of Hubble type. Furthermore, studies of the abundance gradients across Hubble types will need to compare the fractional radii of H II regions using an appropriate radial normalization which is independent of Hubble type. As this paper was being revised for publication, new work by Vila-Costas & Edmunds (1992) came to our attention. This comprehensive analysis of the extant data for disk galaxy abundances is in agreement with our conclusions regarding the abundances and gradients as a function of Hubble type. They also find that barred spirals tend to have shallower slopes than their nonbarred counterparts.

The nebular models presented here confirm that the densities of H II regions significantly affect the strength of the emission lines at high abundances, due to the competition between collisional and radiative de-excitation in the nebular cooling transitions. However, while this effect is important, it does not cripple the use of R_{23} as an abundance indicator. Uncertainty in the ionizing radiation field remains a dominant source of uncertainty in the determination of abundances from the R_{23} ratio.

In summary, our modeling shows that although R_{23} becomes less reliable as an abundance indicator at low excitation, the estimates of the oxygen abundances for our sample of objects are probably still reliable to at least a factor of 2. The result that the abundances for our sample of early-type spiral galaxies are systematically higher than in late-types confirms the trend of previous findings (e.g., Edmunds & Pagel 1984; Smith 1975), but in galaxies of types even earlier than Sb. However, it is also consistent with the findings of Garnett & Shields (1987), who discovered that the H II regions in M81, an Sab galaxy as typed in the RC2, are not substantially different in character than those of late-type galaxies. Our study reveals a large scatter from galaxy to galaxy in the excitation, and presumably abundances, of early-type galaxies as a class.

We gratefully acknowledge Greg Shields for several useful discussions and suggestions on this project, and for the use of his photoionization program. We also thank Don Garnett for helpful tips with the program and comments on a preliminary version of this paper. Thanks also to Ian Evans for providing the numbers and code for the Dopita & Evans (1986) abundance calibration, and to Evan Skillman for useful comments and discussions. Dennis Zaritsky kindly supplied helpful comments on the final draft, and we also thank the anonymous referee. M. S. O. acknowledges with thanks a fellowship from the Zonta International Foundation. This work was supported by the National Science Foundation, through grants AST 89-96123 and AST 90-19150.

REFERENCES

Aller, L. H. 1987, in Spectroscopy of Astrophysical Plasmas, ed. A. Dalgarno & D. Layzer (Cambridge: Cambridge Univ. Press), 89
Baldwin, J. A., Ferland, G. J., Martin, P. G., Corbin, M. R., Cota, S. A., Peterson, B. M., & Slettebak, A. 1991, ApJ, 374, 580
Belley, J., & Roy, J.-R. 1992, ApJS, 78, 61
Bland-Hawthorn, J., Sokolowski, J., & Cecil, G. 1991, ApJ, 375, 78
Caldwell, C. N., Kennicutt, R. C., Schommer, R. A., & Phillips, A. 1991 ApJ, 370, 526
de Vaucouleurs, G., de Vaucouleurs, A., & Corwin, H. G. 1976, Second Reference Catalogue of Bright Galaxies (Austin: Univ. Texas Press) (RC2)
Díaz, A. I. 1989, in Evolutionary Phenomena in Galaxies, ed. J. E. Beckman & B. E. J. Pagel (Cambridge: Cambridge Univ. Press), 377
Díaz, A. I., Terlevich, E., Vílchez, J. M., Pagel, B. E. J., & Edmunds, M. G. 1991 MNRAS, 253, 245
Dinerstein, H. L. 1990, in The Interstellar Medium in External Galaxies, ed. H. A. Thronson & J. M. Shull (Dordrecht: Kluwer), 257
Dopita, M. A., & Evans, I. N. 1986, ApJ, 307, 431
Dufour, R. J., Talbot, R. J., Jensen, E. B., & Shields, G. A. 1980, ApJ, 236, 119
Edmunds, M. G., & Pagel, B. E. J. 1984, MNRAS, 211, 507
Evans, I. N. 1991, ApJS, 76, 985

Evans I. N., & Dopita, M. A. 1985, ApJS, 58, 125
———. 1987, ApJ, 319, 662
Ferrini, F., & Galli, D. 1988, A&A, 195, 27
Fisher, J. R., & Tully, R. B. 1981, ApJS, 47, 139
Galli, D., & Ferrini, F. 1989, A&A, 218, 31
Garnett, D. R., & Shields, G. A. 1987, ApJ, 317, 82
Hayes, D. S., & Latham, D. W. 1975, ApJ, 197, 593
Helou, G., Salpeter, E. E., & Terzian, Y. 1982, AJ, 87, 1443
Hodge, P. W., & Kennicutt, R. C. 1982, An Atlas of H II Regions in 125 Galaxies (Univ. Washington, Dept. of Astronomy)
Huchtmeier, W. K. 1982, A&A, 110, 121
Huchtmeier, W. K., & Richter, O.-G. 1989, A General Catalog of H I Observations of Galaxies (New York: Springer)
Huchtmeier, W. K., & Seiradakis, J. H. 1985, A&A, 143, 216
Hummer, D. G., & Mihalas, D. M. 1970a, MNRAS, 147, 339
———. 1970b, JILA Rep. No. 101
Kennicutt, R. C. 1984, ApJ, 287, 116
———. 1988, ApJ, 334, 144
———. 1989, ApJ, 344, 685
Kennicutt, R. C., Edgar, B. K., & Hodge, P. W. 1989, ApJ, 337, 761
Kennicutt, R. C., Keel, W. C., & Blaha, C. A. 1989, AJ, 97, 1022
Kurucz, R. L. 1979, ApJS, 40, 1
Lacey, C. G., & Fall, S. M. 1985, ApJ, 290, 154
Leitherer, C. 1990, ApJS, 73, 1
Massey, P., Strobel, K., Barnes, J. V., & Anderson, E. 1988, ApJ, 328, 315
Mathis, J. S. 1986, PASP, 98, 995
McCall, M. L. 1982, Ph.D. thesis, Univ. Texas
McCall, M. L., Rybski, P. M., & Shields, G. A. 1985, ApJS, 57, 1 (MRS)
McGaugh, S. S. 1991, ApJ, 380, 140
Mollá, M., Díaz, A., Ferrini, F., & Pardi, C. 1992, in Proc. Elba Workshop, Star-Forming Galaxies and Their Interstellar Medium (1992 June 1–6), in press
Nishimura, M., Kaneko, N., & Toyama, K. 1984, A&A, 130, 46
O'Dell, C. R., & Castañeda, H. O. 1984, ApJ, 283, 158
Osterbrock, D. E. 1989, The Astrophysics of Gaseous Nebulae and Active Galactic Nuclei (Mill Valley: University Science Books)
Pagel, B. E. J., & Edmunds, M. G. 1981, ARA&A, 19, 77
Pagel, B. E. J., Edmunds, M. G., Blackwell, D. E., Chun, M. S., & Smith, G. 1979, MNRAS, 189, 95
Peimbert, M. 1975, ARA&A, 13, 113
Peterson, S. D. 1979, ApJS, 40, 527
Pogge, R. W. 1988, ApJ, 328, 519
Rots, A. H. 1974, Ph.D. thesis, Univ. Groningen
Sandage, A., & Tammann, G. A. 1987, A Revised Shapley-Ames Catalog of Bright Galaxies (2d ed.; Washington: Carnegie Institution) (RSA)
Schild, R. E. 1977, AJ, 82, 337
Scowen, P. A., Dufour, R. J., & Hester, J. J. 1992, AJ, 104, 92
Searle, L. 1971, ApJ, 168, 327
Shields, G. A. 1990, ARA&A, 28, 525
Shields, G. A., & Searle, L. 1978, ApJ, 222, 821
Shields, G. A., Skillman, E. D., & Kennicutt, R. C. 1991, ApJ, 371, 82
Shields, G. A., & Tinsley, B. M. 1976, ApJ, 203, 66
Shostak, G. S. 1978, A&A, 68, 321
Skillman, E. D., Melnick, J., Terlevich, R., & Moles, M. 1988, A&A, 196, 31
Smith, H. E. 1975, ApJ, 199, 591
Stasińska, G. 1990, A&AS, 83, 501
van der Hulst, J. M., Kennicutt, R. C., Crane, P. C., & Rots, A. H. 1988, A&A, 195, 38
Viallefond, F. 1985, in Star Forming Dwarf Galaxies & Related Objects, ed. D. Kunth, T. X. Thuan, & J. Tran Thanh Van (Paris: Éditions Frontières), 207
Vila-Costas, M. B., & Edmunds, M. G. 1992, MNRAS, 259, 121
Vílchez, J. M., & Pagel, B. E. J. 1988, MNRAS, 231, 257
Zaritsky, D., Elston, R., & Hill, J. M. 1990, AJ, 99, 1108
Zaritsky, D., Kennicutt, R. C., & Huchra, J. P. 1993, in preparation